Mineral Characterization Using Scanning Electron Microscopy (SEM)

Subjects: Materials Science, Characterization & Testing

Contributor: Asif Ali , Ning Zhang , Rafael M. Santos

Scanning electron microscopy (SEM) is a powerful tool in the domains of materials science, mining, and geology owing to its enormous potential to provide unique insight into micro and nanoscale worlds. The rapid pace of technological development requires a detailed study of minerals to a further extent to meet the unprecedented material demands of the evolving world. There are more than 5956 species of minerals known today, and the number of new identifications is evolving, with as many as 50 new types identified each year. Quantitative measurements and qualitative analyses of mineral compositions within mining ores and reservoirs have valuable importance with practical applications. Comprehensive and accurate information can be gathered for the identification of rocks and minerals, including structural characteristics and mineral composition, which can provide worthy information about pore structure and reservoir heterogeneity.

scanning electron microscopy | minerals | artificial intelligence | machine learning | energy-dispersive spectrometer | secondary electron imaging

1. Scanning Electron Microscopy and Mineral Characterization

SEM makes use of secondary electron imaging to analyze the surface topology and morphology of micron/nanometer-scale minerals [1]. For a comprehensive understanding of the microstructure and mineral components, SEM is usually combined with X-ray techniques to complement the acquired information [2][3][4][5]. The infrared spectroscopy method is helpful in identifying chemical species and determining the molecular structure of minerals. This technique has been widely used in mineral characterization [6][7][8][9].

One of the major quantitative analysis methods in mineral analysis is X-ray diffraction (XRD). It correlates the content of minerals with diffraction density, which helps in identifying and quantifying the minerals present in the sample [10][11]. For example, XRD can be used to analyze calcite and nahcolite in saline brine [12], evaluate deposits by identifying minerals in phyllite [13], examine the order degree of dolomite [14], and study the content of calcite and dolomite in carbonate rocks [15]. XRD is a rapid and accurate method for quantitative mineral analysis; however, some mineral compositional structures could lead to errors in analytical results [10].

Combining qualitative analysis with quantification assessment methods can provide a better understanding of the investigated minerals. Such methods include SEM energy-dispersive spectroscopy (SEM–EDS) [15][16][17][18][19],

automated SEM mineral liberation analysis (SEM-MLA) [20][21][22], and quantitative evaluation of minerals by scanning electron microscopy (QEMSCAN) [23][24][25]. These methods incorporate a mineral quantitative analysis system by using an energy spectrometer and SEM. For accurate identification of minerals, backscattered electron (BSE) images are used, which can reflect the difference between the X-ray energy spectrum and mineral phase composition [26][27][28]. The quantitative analysis of rare earth minerals is a challenging task with conventional identification methods, and the abovementioned techniques have attained rare earth mineral identification. The problems associated with the usage of these methods pertain to difficulties in application, promotion, and high measurement costs.

1.1. SEM Energy-Dispersive X-ray Spectroscopy (SEM–EDS)

When the electron beam emitted from the gun penetrates and interacts with the volume beneath the sample surface, X-rays are generated. This is a well-established principle in physics: the deceleration of electrons due to their entrance into the Coulomb field of the specimen results in a loss of electron energy and emits photons. In SEM analysis, similar X-ray photons are emitted, which are characteristic of the sample under investigation [26].

The quantification scheme is achieved by measuring the X-ray intensity. This was illustrated by Heinrich and Yakowitz in 1968 in their publication, *Quantitative Electron Probe Microanalysis* [29], which later became the standard for developing X-ray fields. At that time, X-ray absorption, determination of correction factors at the instant of electron penetration and scattering, and conversion of X-ray intensity to the relative concentration were missing. Many problems pertaining to the electron probe field were solved with the development of energy-dispersive spectrometry (EDS). At present, various studies have incorporated SEM–EDS for qualitative and semiquantitative analysis in a variety of subject areas [30][31][32][33][34][35][36].

A schematic diagram of an energy-dispersive spectrometer is shown in **Figure 1**. The X-ray detection system (which is a solid-state detector) separates the characteristic X-rays of various elements present in the sample. Then, the EDS system software analyzes the energy spectrum to determine the amplitudes of particular elements, and electrical signals are generated from the respective photon energies. This results in qualitative and quantitative determination of a chemical composition map of the elements present in the sample [26]. SEM–EDS has been used in a variety of fields for mineral characterization [37][38][39][40][41][42][43].

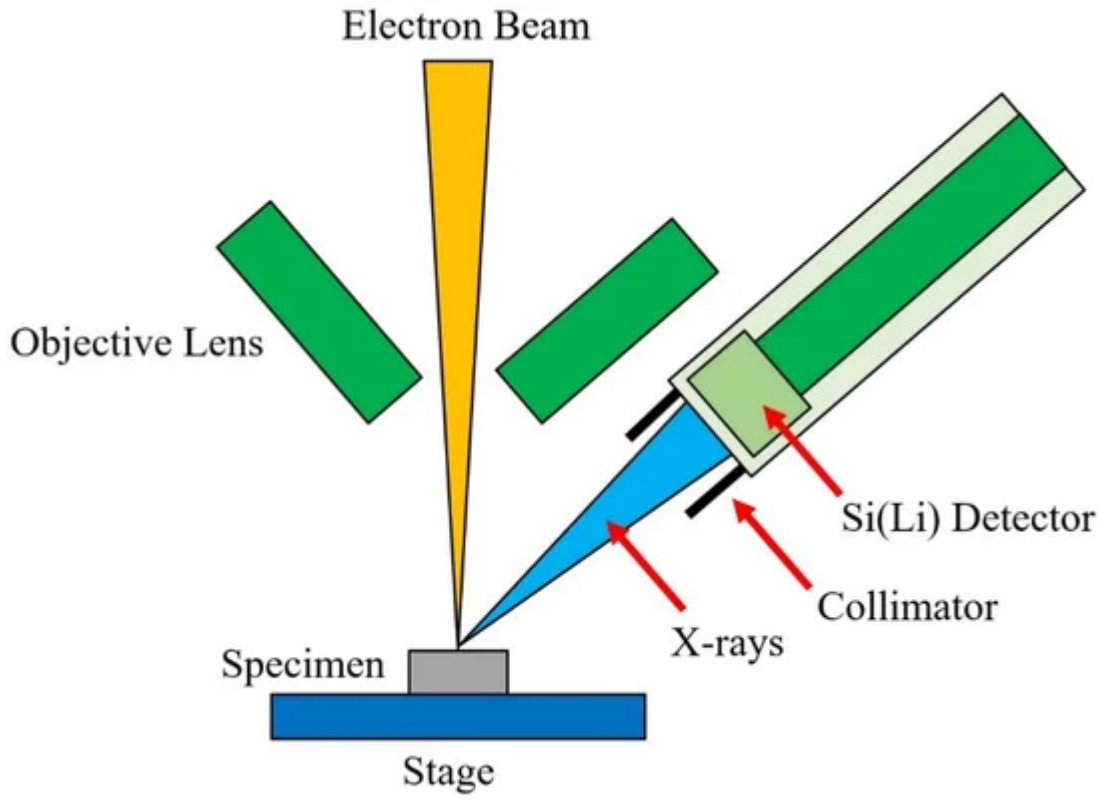

Figure 1. Schematic diagram of an energy-dispersive spectrometer.

1.2. SEM-Based Automated Mineralogy (SEM-AM)

SEM-AM is a tool that was initially designed to characterize mineral processing products and ores. The measurement process starts with collecting backscattered electron (BSE) images, which are analyzed using image analysis software procedures. Based on BSE image adjustments, the energy-dispersive X-ray spectra (EDS) are obtained at selected points. The EDS spectra of the sample are then classified based on the list of approved reference EDS spectra. Relevant software providers offer services such as particle analysis, EDS spectral mapping, sparse phase search, and point counting modal analysis using four principal SEM-AM measurement routines and different classification algorithms, which can be used based on the analysis requirements. The main challenges associated with the process are materials with very different hardnesses, polishing relief surfaces of particles, electron beam stability, and appropriate nonevaporating epoxy resin mixtures [21].

SEM-based automated mineralogy (SEM-AM) is still underutilized, although SEM instruments are widely distributed in industry, geosciences, and materials research. SEM-AM can produce valuable results for a variety of major applications by characterizing the primary ores and optimizing mineral concentration, flotation, comminution, and metallurgical processes in the mining industry through the generation of quantified reliable data [44][45][46][47][48]. Beyond the classical fields, the potential of SEM-AM has gained further interest on scientific and economic grounds. Some closely related topics are ore fingerprinting, metallurgy, and applications in petrology [49][50][51].

SEM-AM systems are a combination of hardware platforms, processing software, and specific image analysis. Any SEM with minor adjustments can be used as a hardware tool for SEM-AM. These adjustments include a high

vacuum operation mode and additional internal mainboards. A vacuum pressure of 10^{-5} to 10^{-7} Pa is needed for its operation. Electron sources of tungsten cathodes and field emission guns can be employed. Tungsten cathodes can be used for economical operation; however, field emission guns are recommended for the long-term stability of electron beams for automated measurements. The speed of analysis and X-ray count rate are increased in SEM-AM by employing two or more EDS spectrometers in the SEM hardware. Multiple samples can be accommodated in a large sample chamber for simultaneous analysis in a single measurement session. A very accurate stage movement of SEM allows precise positioning using small intervals. For valuable analysis results, a fine-quality backscattered electron (BSE) detector is needed. In SEM-AM analysis, BSE image quality and stability are important factors, as the resultant image (in combination with the EDS spectrum) is used for phase or mineral discrimination. Prior to measurement, fixed working distances must be set to keep the BSE image gray levels constant [21].

Keeping the image calibration constant ensures that a specific phase or mineral always possesses the same BSE image gray level. The calibration process can be conducted with various BSE image gray levels of reference materials such as quartz (dark gray), copper (intermediate), and gold (very bright) [21]. The choice of calibration reference material should be made based on the sample material to be investigated. For example, many slags, industrial ash, or particulate materials are investigated using SEM-AM, and quartz or copper are used for calibration with dark gray to intermediate BSE image gray levels. This results in SEM images with better resolution and quality. For SEM-AM technology, four principal measurement routines can be outlined, which starts with collecting BSE gray-level images with respect to the calibrated gray level, as shown in **Figure 2**. The upper row represents the BSE images, while the bottom row indicates the EDS images of SEM-AM of one measurement frame. White or black crosses denote the points of X-ray analyses (only some points are shown). **Figure 2** presents the EDS point counting technique used for the quantification of modal composition. **Figure 2** shows particle analysis by EDS, which has been developed for fast automated characterization of grain mounts with up to 10^6 particles, such as milled products from mineral processing and mining. **Figure 2** illustrates the sparse phase search method, which combines single spot EDS spectral analysis of grains with a BSE gray tone value trigger. It is valuable in massive rock applications, such as drill cores and thin sections. **Figure 2** demonstrates EDS spectral mapping, which combines BSE image levels with mapping of the EDS spectrum. This method is helpful, especially in cases where fine details of mineral intergrowth are considered. In summary, SEM-AM is a powerful tool for mineral characterization and has actively been used in recent literature [52][53][54][55].

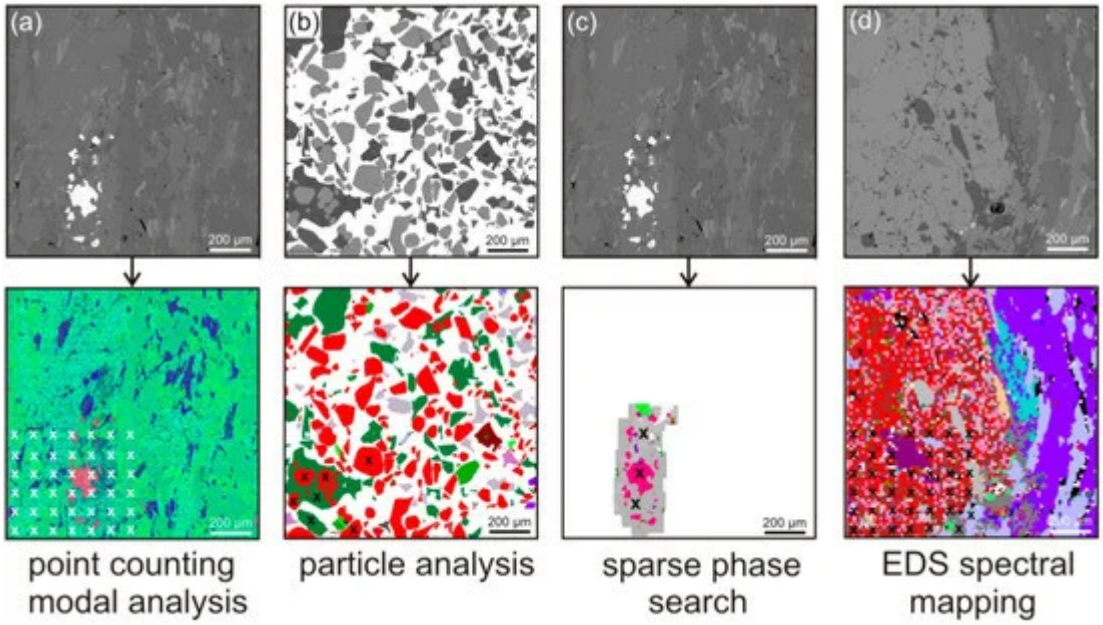

Figure 2. SEM-AM methods of one measurement frame showing BSE (**upper row**, **a**–**d**) and EDS (**lower row**) images. Numerous single EDS analysis points map each grain with a distinguishable BSE gray level and are visualized as color-coded pixels, such as the garnet grain, which is indicated by red-colored pixels [21]. CC-BY.

1.3. Automated SEM Mineral Liberation Analysis (SEM-MLA)

Recent software developments in SEM have incited dominant growth in its application in solid matter investigations. One of the economic solutions is the use of mineral liberation analysis (MLA) for optimizing the mineral processing methodology of metallic ores. SEM-MLA has been an important driver in transforming numerous software versions for SEM applications [21]. SEM-MLA was designed to quantify the mineralogy of ores. After the mining process, the ore is processed to increase the concentration of minerals of interest (and value). The processing of ores is also important for removing minerals of no value or those with detrimental effects on the needed mineral products. This processing of grinding the ores and liberating the minerals of interest provided rapid automated analysis of target minerals and extensively improved the process.

A mineral liberation analyzer (MLA) based on SEM was developed in the late 1990s by the JKRMC (Julius Kruttschnitt Mineral Research Centre, Australia), and it is currently commercially available [55]. In MLA, minerals are differentiated by attaining and combining the information gathered from EDS and BSE. Depending on the size range of the particles in the sample, size fractions from the sample are produced. Then, liberation is measured in each size fraction, followed by liberation reconstruction of the whole sample. The measurement of mineral liberation is usually carried out through one of two methods, i.e., either the area method or the linear intercept method. Liberation by area measurement has shown lower stereological error compared to linear measurement.

It is important to note that liberation measurements by the linear intercept method are known as one-dimensional, while area method measurements are called two-dimensional liberations. Both of the measured liberations are lower dimensional projections of the true volumetric liberation, which is three-dimensional. Stereological correction

is based on stereological transformation and prediction of liberation measurements. This stereological correction can be based on entropy regularization [56]. Correction of the apparent liberation and production of three-dimensional liberations have also been described in several other investigations [57][58][59]. Various operating modes for the MLA system are available, i.e., X-ray modal analysis (XMOD), particle X-ray mapping (PXMAP), selected particle X-ray mapping (SXMAP), sparse phase liberation analysis (SPL), standard BSE liberation analysis (BSE), extended BSE liberation analysis (XBSE), and rare phase search (RPS) [60]. The use of SEM-MLA is shown in **Figure 3** for quantifying the mineralogy of a hydrothermally overprinted alkali plutonite [22].

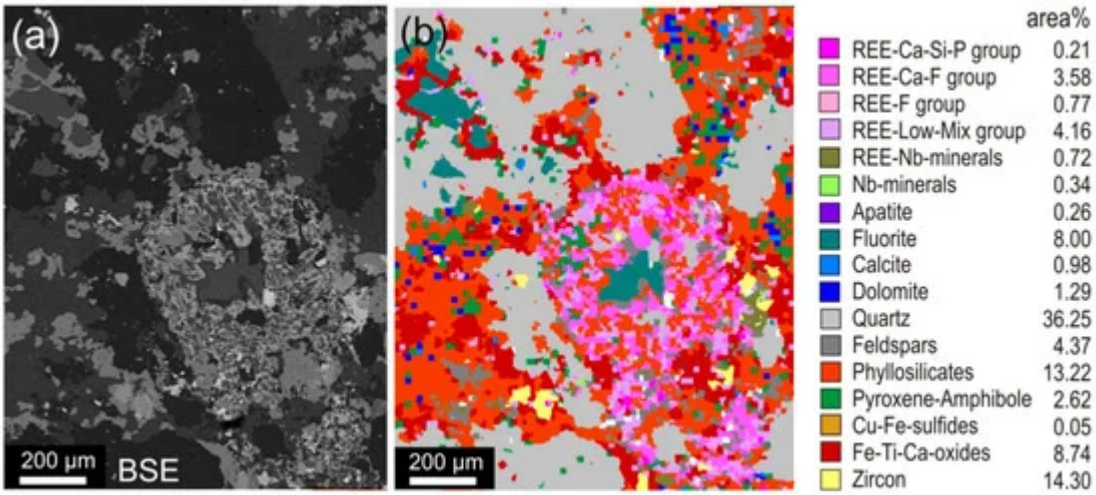

Figure 3. (**a**) SEM-MLA measurement of a hydrothermally overprinted alkali plutonite showing the backscattered electron (BSE) image and (**b**) color-coded, grouped, and classified presentation of the frame presented in (**a**) [22]. CC-BY.

1.4. Quantitative Evaluation of Minerals by Scanning Electron Microscopy (QEMSCAN)

Traditional mineral analysis based on microscopy cannot provide the needed data because of the absence of quantitative information and the very small size of the particles of interest. QEMSCAN technology, initially termed QEM*SEM, demonstrated the potential to revolutionize automated mineralogy [61]. In a mold, the particulate mineral sample is mixed with epoxy resin, and the sample surface is prepared using cutting, polishing, and carbon coating. The sample is scanned using SEM in backscatter mode, enabling the differentiation of particles from the background. After the identification of particles on the resin block, their composition is systematically mapped using EDS. In contrast to the most modern SEMs coupled with single EDX, QEMSCAN possesses the attribute of having multiple EDXs at the same time, enabling rapid quantitative mineralogy. The acquired EDX signals are then compared with reference known materials in the database and assigned a mineral name or to a chemical compositional grouping. With this process, the mineralogy of the sample can be determined by particle-by-particle analysis [61]. QEMSCAN locates the particles using a BSE signal, while identifying the mineral by an EDS signal. It can be compared to SEM-MLA, which makes more use of the BSE signal than EDS for identifying the mineral. SEM-MLA works very well for bright phases (such as platinum group element minerals).

Among SEM–EDS techniques, QEMSCAN is one of the most widely used and offers quantitative characterization of minerals, ores, and other mineralogical compounds [62][63][64][65][66]. QEMSCAN is usually used in conjunction with other analytical techniques, such as electron probe microanalysis (EPMA) and X-ray diffraction (XRD), as shown in **Table 1** [67]. **Figure 4** indicates the use of QEMSCAN for identifying the mineral distribution of four samples [67]. It shows the presence of geothite, quartz, clay, limonite, and other silicate minerals.

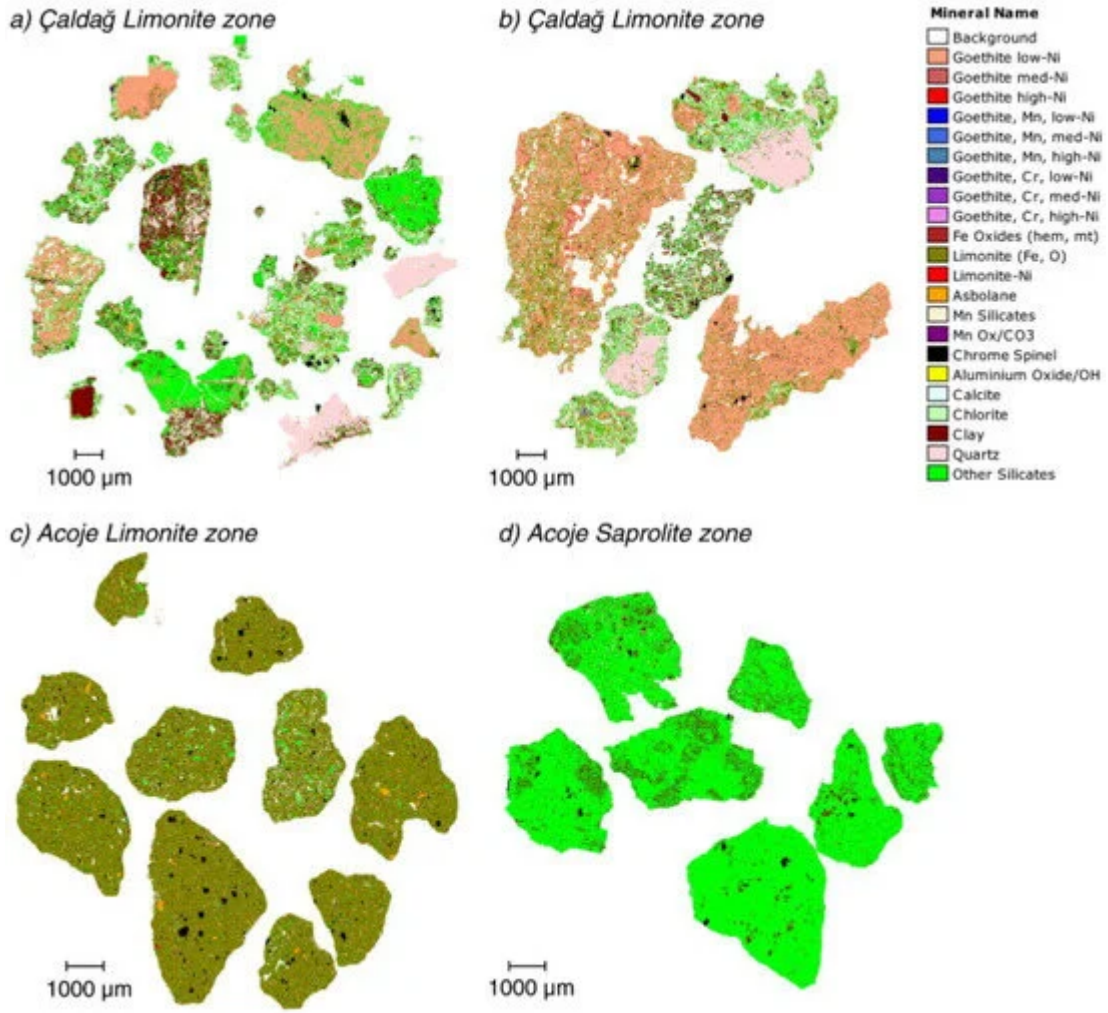

Figure 4. QEMSCAN analysis indicating mineral distribution in four different zones [67]. CC-BY.

Table 1. Techniques used for investigating mineralogy and their comparison. ✔ indicates good, ● represents poor, while ▲ suggests it is possible but not recommended [67].

Investigation	Electron Microprobe	XRD	QEMSCAN
Mineral texture	▲	●	✔✔✔
Mineral distribution and associations	▲	●	✔✔
Mineral-specific particle size information	▲	●	✔✔
Mineral abundance	●	✔✔✔	✔✔✔

Investigation	Electron Microprobe	XRD	QEMSCAN
Amorphous minerals (geothite, silica)	✔✔✔	●	✔✔✔
Distribution of minor metals within minerals	✔✔✔	●	✔
Crystallinity (clay, silica, geothite, and limonite)	●	✔✔✔	●

M

The advancement of SEM with automated mineralogy has provided a quick and relatively economical quantitative mineral analysis solution. However, the absence of statistical errors makes the robustness of the results uncertain. This could damage the reliability of technical solutions taken on the onus of these quantitative outcomes [68]. Automated mineralogy-based measurements have been studied with several methods for the estimation of uncertainties. For instance, a statistical approach was developed by Benvie et al. in 2013 for using SEM automated mineralogy in accordance with diagnostic leaching tests [69]. It was concluded that to derive the standard deviation and background variance, at least two grain mount measurements were needed for each head and leach residue sample. In another study, the variability in mineral liberation analyses and mineral quantity was investigated by Lastra and Paktunc in 2016 [70]. They studied the fraction of sulfide flotation rougher concentrate of −509 to 208 µm in size through interlaboratory testing. Mineral quantities were found to have good agreement with the data, but mineral association and liberation analyses showed less agreement. This finding hints toward the idea that correct mineral liberation and association may not necessarily be found with correct mineral quantities. In 2021, Guseva et al. evaluated the analytical errors in mineralogical measurements by applying the point counting method via binomial distribution approximation [71]. Binomial approximation may not fit well with all cases, especially with coarse materials, and suitable methods for each case should be used, such as estimation of the confidence method [72] or the bootstrap resampling method [73].

The estimation of errors in textural characteristics measured by automated mineralogy can be efficiently identified using the bootstrap resampling method [74]. For instance, the bootstrap approach can help in evaluating the uncertainties related to particle properties measured by SEM automated mineralogy for the evaluation of magnetic separation efficiency [75][76], density separation processes [77], and the simulation and statistical modeling of mechanical separation processes [78]. The bootstrap resampling method considers a population of *N* samples, takes *M* random subsets, and replaces the randomly selected samples to ensure that the entire population is available for sampling [79][80]. The accepted statistical methods, which use the point counting method on polished sections and assess errors in mineral grades, agree well with the bootstrap method [81][82][83]. This method has the advantage of being assumption-free and can be applied to a wide range of particle characteristics [73]. It does not assume a bionomical distribution. These methods imply that the standard deviation of mineral grades is proportional to the square root of the number of particles measured or the total area of particles measured. The relative standard deviation of measurements for any mineral grade can be estimated as follows [84]:

$$RSD = ax^{-0.5}$$

where RSD is the relative standard deviation, a is a coefficient, and x is the mineral grade.

The bootstrap method can also provide information about the measurement of how much total area (grains) is needed to reach a given uncertainty. In addition to the uncertainty, SEM also has some drawbacks, including (but not limited to) limited depth of penetration that primarily provides surface information; and low accelerating voltages that provide low-resolution images, while increasing the voltage starts damaging the surface of the sample.

2.1. Constraints in Phase Identification by EDS Spectra

It is a common claim in SEM-based automated mineralogy studies that minerals can be detected, identified, and quantified by their characteristic EDS spectrum (an example is shown in **Figure 5**, indicating feldspar mineral albite [21]). However, this claim cannot be fully correct, as minerals are characterized by their lattice structure indicated by XRD first, and then comes the use of elemental composition information provided by EDS spectrum quantification. Therefore, mineral identification remains incomplete with use of the EDS spectrum only, based on its foundations on elemental composition. Identifying a mineral by chemical composition alone can be misdirecting, as there are examples of minerals with similar chemical compositions but different crystal structures based on the crystallization conditions of minerals. For instance, pseudorutile and ilmenite are both titanium-iron oxide minerals, but they exhibit different crystal structures [21].

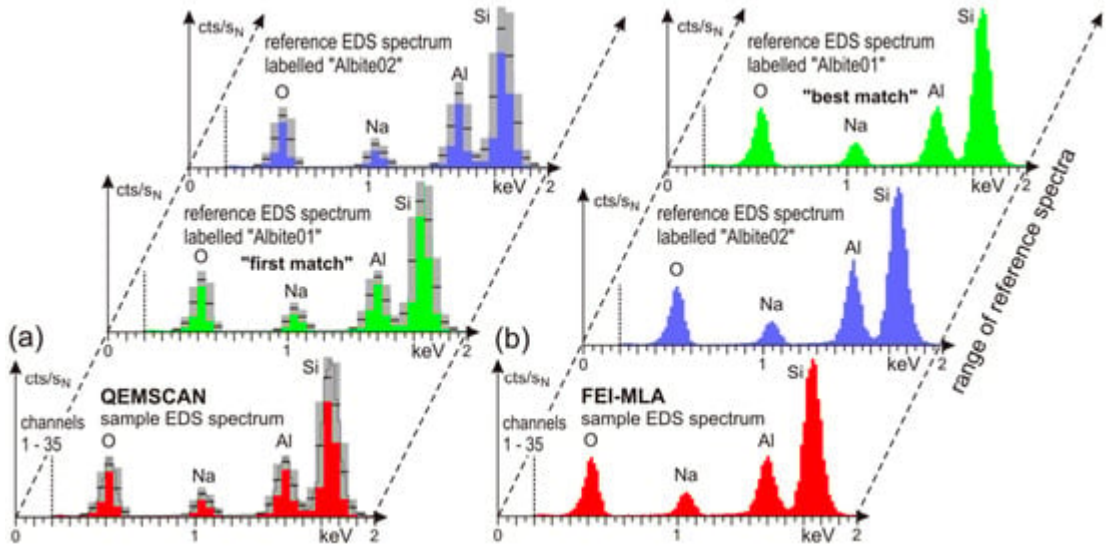

Figure 5. Classification modes of EDS spectra: (**a**) FEI-QEMSCAN, and (**b**) FEI-MLA for feldspar mineral albite [21]. CC-BY.

Another challenge in mineral detection, identification, and distinction using EDS spectra is that some minerals have very similar elemental compositions, such as hematite (Fe_2O_3) and magnetite (Fe_3O_4). Hematite is composed of 70% by weight Fe and 30% by weight O, while magnetite is made up of 72% by weight Fe and 28% by weight O. The EDS spectra for both minerals appear to be very similar, and the very trivial differences in Fe and O peaks cannot be resolved by appearance. In such scenarios, it is a good idea to use the BSE image gray level as an additional distinguishing standard. It must be noted that for such a measurement, a specific BSE brightness and contrast calibration is needed. Another challenge is the detection range of EDS spectra, as it does not cover the whole elemental periodic system. For example, the first light elements cannot be detected by EDS, such as H, He,

Li, and Be. It is, therefore, recommended to complement EDS spectra with XRD and XRF methodologies for mineral identification and quantification [21]. Other limitations of EDS spectra include longer mapping causing damage to the samples, low sensitivity of light elements, low quantitative accuracy, information about the chemical composition only (not about functional groups or chemical bonds), and overlapping peaks, making it difficult to distinguish among elements present in the sample.

2.2. Sample Preparation and Related Issues

For the success of any SEM analysis, an optimal sample preparation process is essential. A wide variety of samples can be analyzed using SEM. The configuration of the sample holder system and the size of the SEM sample chamber are the defining parameters for choosing the type of sample for investigation. Grain mounts in round epoxy blocks are usually used for particulate or granular samples. If the samples are massive and contain compact matter, such as rocks, petrographic glass-mounted sections can be used. Depending on the type of sample, the production of thin grain mounts on glass is also possible. Two important configurations must be maintained, whether they are samples on glass or round block sample holders, i.e., the holder should be mounted perpendicular to the electron beam and parallel to the BSE detector [21].

Grain mounts in epoxy blocks are the best form to prepare samples if the sample material is noncompact, particulate, or granular, which can be ground, hand-picked single, or broken grains [85]. A potential problem occurs when the grains are not easily separated within the same colored grayscale BSE image, as most SEM-AM software packages are unable to distinguish between them. The use of pure graphite is beneficial in such cases, as it can be utilized in stirred form as a distance material into epoxy resin blocks [85]. In some granular sample cases, a wide range of densities can exist among the phases present in the sample. During the stirring process of sample grains with graphite-saturated epoxy resins, grains with larger sizes and high densities tend to move toward the bottom of the holding block, and it is more probable that small grains will be missed in the analysis. One good practice for dealing with such kinds of samples is cutting round blocks into vertical slices, which can be remounted as vertical sections [21]. It is also possible to study other materials, such as polymers and coal, with the use of EDS detectors. Since the BDE gray value of this organic matter is similar to that of epoxy resin, an alternative embedding material should be used [86]. Carnauba wax is an alternative material that can be used for embedding in these cases [87]. Carnauba wax is a very soft material, making it difficult to polish. One possible solution is to double-mount the Carnauba wax in epoxy resin blocks. Another prospective solution could be the doping of iodoform in epoxy resin [86][88]. The organic matter has a lower atomic number than the epoxy resin, which makes the epoxy a background material. A wide variety of epoxy resins are available for this purpose [89]. SEM images of some epoxy resins and their respective thermal conductivities are shown in **Figure 6**. In addition to the variety, the proportions of hardener and filler can be varied. The challenges in choosing an epoxy resin are that it must remain stable under a 25 kV electron beam, not evaporate under high vacuum conditions, and harden within convenient temperature conditions and time frames. The recommended approach to solving such problems is continuous application tests.

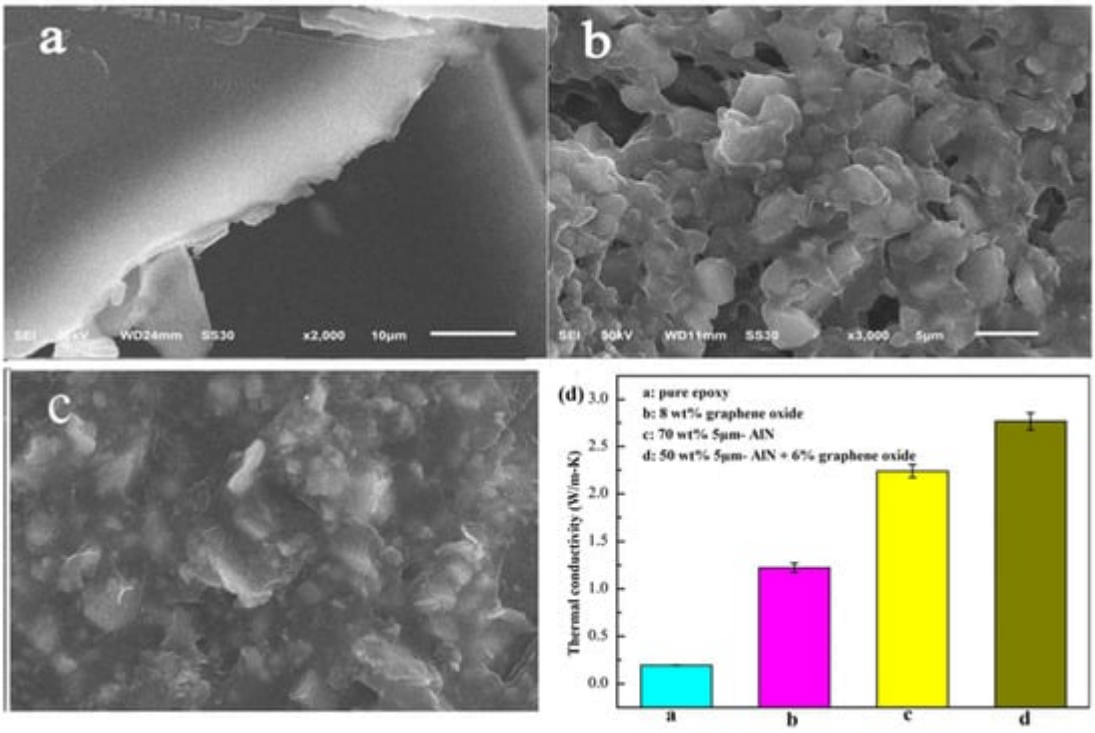

Figure 6. Epoxy adhesives shown using SEM with (**a**) epoxy resin only, (**b**) epoxy resin with aluminum nitride particles, (**c**) epoxy resin with aluminum nitride and graphene oxide, and (**d**) the thermal conductivities of various test samples. [89][90]. Re-used with permission (5673961270857) from Elsevier (**a–c**) and CC-BY (**d**).

The complications associated with the sample preparation procedure depend on the type of sample material. If it is solid, dry, compact, and massive, the preparation of thin and thick sections is quite simple. In the case of brittle and/or porous material, epoxy resin is impregnated with a previous material for stabilization before sawing. Thin and thick section production has been reported by several studies [91][92][93]. Usually, silicon carbide (SiC) with 600 to 1000 mesh is used for lapping of the sample material behind the mounting on glass. In the standard lapping procedure, SiC 1000 works best for brittle and soft materials, with minimum substance loss compared to SiC 600. If the sample contains minerals with different optical properties but a closer chemical composition, thin sections are advantageous as an optical microscope can also be used to check the minerals and phases. In addition, a microscope with polarized light can be used to recognize samples with glassy phases owing to their optical isotropy. The reference EDS spectra list can be compiled based on this set of information [21].

A plane and well-polished surface is needed for SEM-AM to analyze grain mounts of thin and thick sections and mounts in epoxy resins. Every material needs a specific treatment, so it is safe to state that the polishing part is a work of craftsmanship. In most cases, water is used in the polishing procedure. If there is a chance of water reacting or mixing with the minerals or materials, the sample preparation procedure can be carried out with water-free liquids such as ethylene glycol [21]. A variety of industrial ashes, such as power plant and sewage ashes, can contain anhydrite, and the use of water-free liquids is recommended in such cases. For samples with varying degrees of particle hardness, covering the polishing plates with hard textile cloth is proposed. Plates covered with soft cloth having long fibers work well for samples containing minerals, soft metals, or ore minerals. The procedure of polishing the sample works well with decreasing grain size, for example, using abrasive papers first, then

grinding, and then polishing powders on textile cloth. It is important to mention avoiding the use of lead-bearing polishing plates for general sample preparation, as it may cause sample contamination with lead. For the last step of sample polishing, the use of diamond powder with diamond paste or lubricant is very effective. The polishing procedure can be controlled using a reflected light microscope to inspect the level of successive polishing steps. The impinging electrons in SEM should be dissipated well to obtain optimal BSE images. The use of carbon coating on polished samples provides a solution, which can be accomplished by either evaporation of carbon-loaded thread, electronic carbon thickness control, carbon rods, etc. [21].

The quality of SEM images in publications is essential for clear communication and interpretation. It is also significant for ensuring reproducibility and avoiding hindrance in future research directions. Blurry SEM images also cause limitations in quantitative data extraction and challenges to peer reviewers in analyzing, interpreting, and understanding the results. Low-resolution images in scientific papers appear for several reasons, some of which may be unintentional, while others are the result of constraints or limitations of the research process. The common reasons for the presence of low-quality SEM images in papers may include (but are not limited to) instrument limitations, sample conditions, resource constraints including time and budget, image processing and acquisition, sample size, scope of the paper, image compression, historical or legacy data, data storage, and file size. To produce focused and clear SEM images for the efficient transfer of information, the stigmator tool in the SEM instrument should be properly utilized.

The stigmator is one of the critical components of the SEM instrument and is responsible for maintaining the astigmatism of the electron beam and adjusting the focus of the SEM equipment. While examining the fine details of mineral structures, astigmatism can cause distorted and blurry images. The stigmator ensures the symmetry and focus of the electron beam, consequently producing quality SEM images. The proper use of a well-adjusted stigmator allows characteristic mineral identification, enhanced elemental analysis, quantitative analysis, and precise imaging of microstructures. It also helps in enhancing images of thin sections and provides crystal clear information about crystal faces, surface roughness, and other textural attributes, which is essential for understanding the formation of minerals and digging deep into the geological history of minerals.

Figure 7 shows wollastonite samples mounted on three stubs. **Figure 8** shows the effects of layers and sputter coating on SEM analysis by comparing wollastonite samples A, B, and C for three magnifications, i.e., 5k×, 60k×, and 250k×. In the sample preparation stage, sample C was left uncoated to investigate the effect of sputter coating, while samples A and B were coated with gold-platinum coating. It is clearly illustrated in **Figure 8** that all SEM images of sample C are fuzzy and dark with few very bright spots and lines, making it difficult to visualize the sample morphology. This is the charging effect, logically occurring due to the absence of a conductive material coating. Another important aspect can be found by comparing the 60k× and 250k× SEM images of sample C with its 5k× image. While charging effects are prominent in all SEM images, that with lower resolution provides better visualization of features when compared to the ones at higher resolution. This suggests that for samples that are difficult to coat with conductive materials, it is useful to capture SEM images at lower resolution. When comparing the SEM images of samples A and B, it is observed that the morphology of the sample can be well studied with single-layered samples compared with multilayered samples.

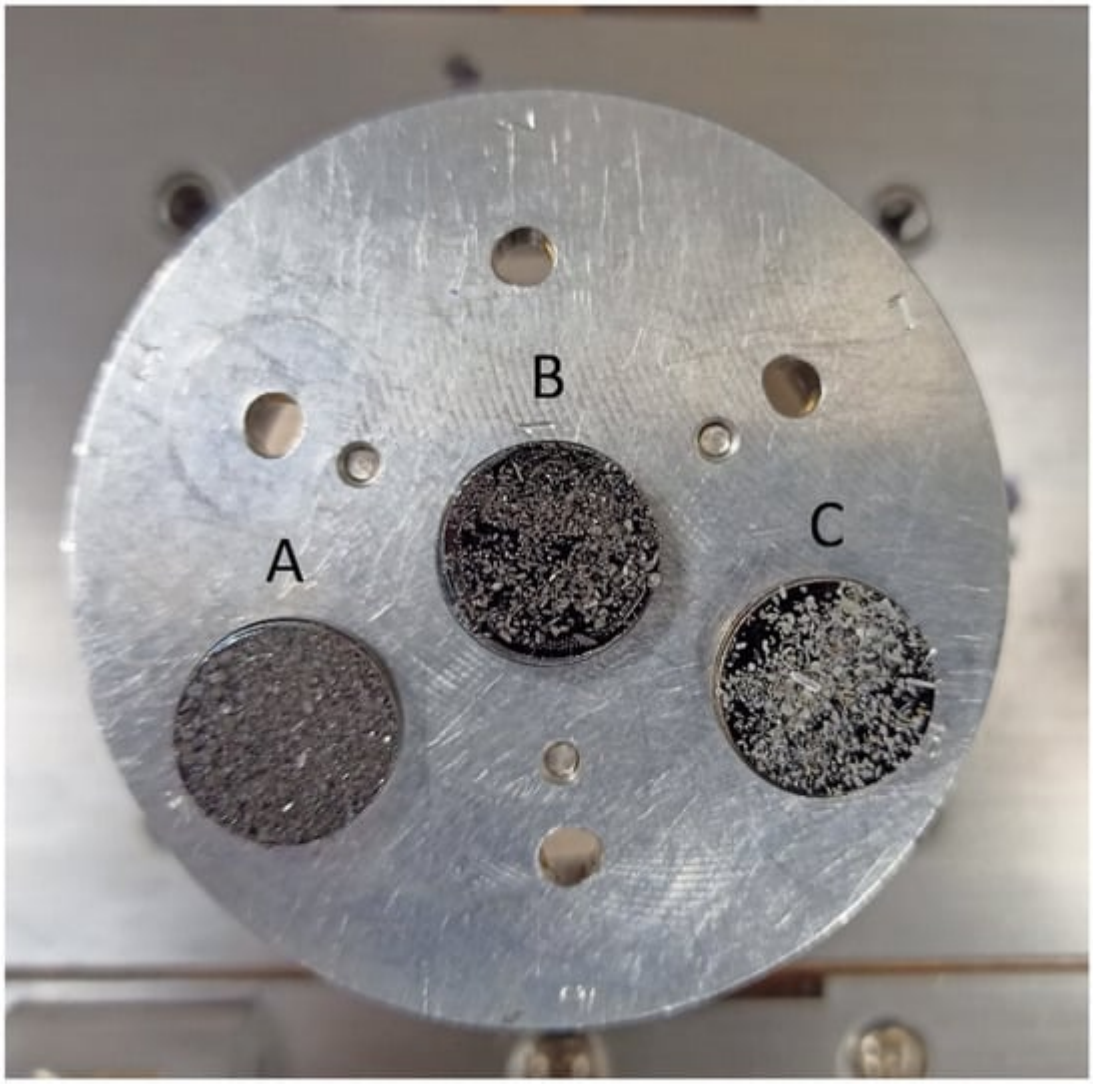

Figure 7. Wollastonite samples prepared for SEM analysis: (A) multilayer, coated; (B) single layer, coated; and (C) single layer, uncoated.

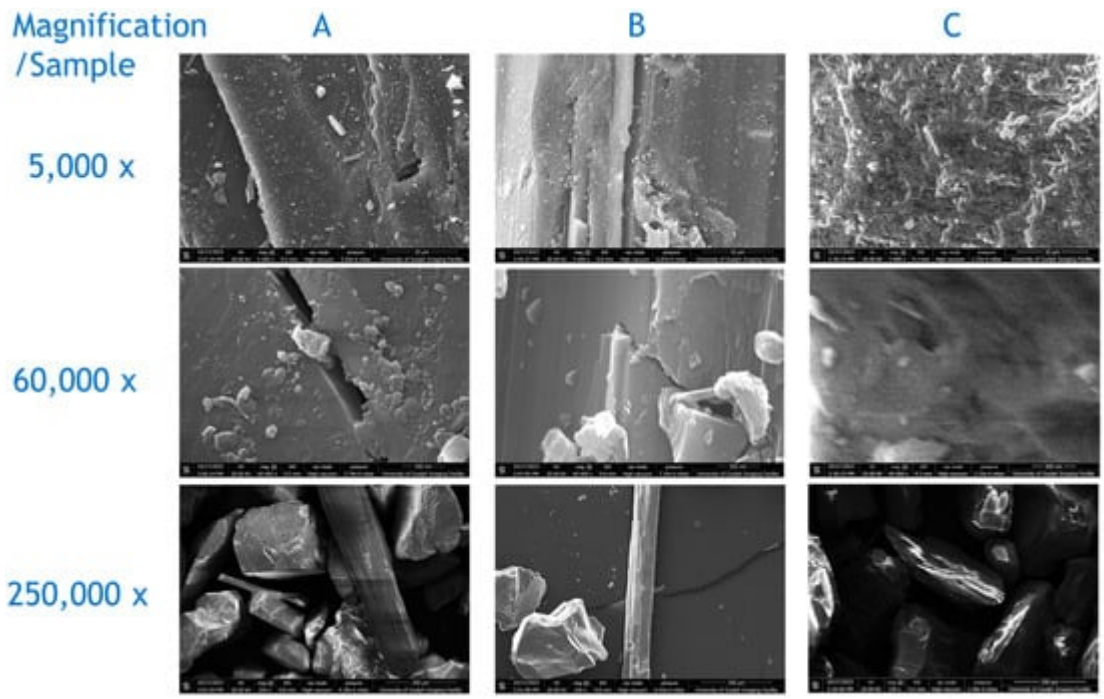

Figure 8. SEM images of wollastonite samples **A**, **B**, and **C** captured at 5k×, 60k×, and 250k× magnifications.

To ensure that the stigmator is well adjusted for taking quality SEM images, the SEM instrument should be allowed to stabilize and warm up, which will ensure that the electron source and other components of the instrument are at steady state before any adjustment. There are usually two stigmation modes in SEM, i.e., objective lens stigmation and condenser stigmation. The specific requirement of the imaging task will require the selection of an appropriate stigmation mode. Misalignment in electron columns and detectors can adversely affect SEM image quality, which is why it is important to ensure proper alignment of these components before starting the imaging process. Some of the latest SEMs include automated alignment features. The sample preparation stage is also important for avoiding any contamination and charging effects hindering image quality. Dry, clean, and well-mounted samples provide a foundation for high-resolution SEM imaging. While focusing the electron beam on the sample, it is necessary to adjust the astigmatism controls to obtain a sharp image at low magnification. It is considered good practice to select a well-defined edge or feature on the investigated sample as a reference point for stigmation control adjustments. Astigmatism is usually indicated by distortions in the SEM image, such as asymmetrical or elliptical features. In the SEM imaging process, it is important to observe such biases. The X- and Y-stigmation (representing horizontal and vertical stigmation, respectively) need to be adjusted to eliminate any distortions. The focus of the electron beam should be rechecked and adjusted, if necessary, for proper and clear imaging. For optimal SEM imaging, several iterative adjustments might be needed. **Figure 9** compares the stigmator adjustment effect on SEM images, which vividly indicates the importance of stigmator adjustment in SEM analysis. Additionally, **Figure 10** shows the effect of maintaining the electron beam for a longer period of time at a single point, which damages the surface of the sample (rectangle marks indicated by dashed circles). This issue can be resolved by reducing the voltage of the electron beam, but that comes at the expense of lower resolution of the SEM image. Therefore, it is recommended to find an optimum voltage–resolution combination that works well for a specific type of sample material.

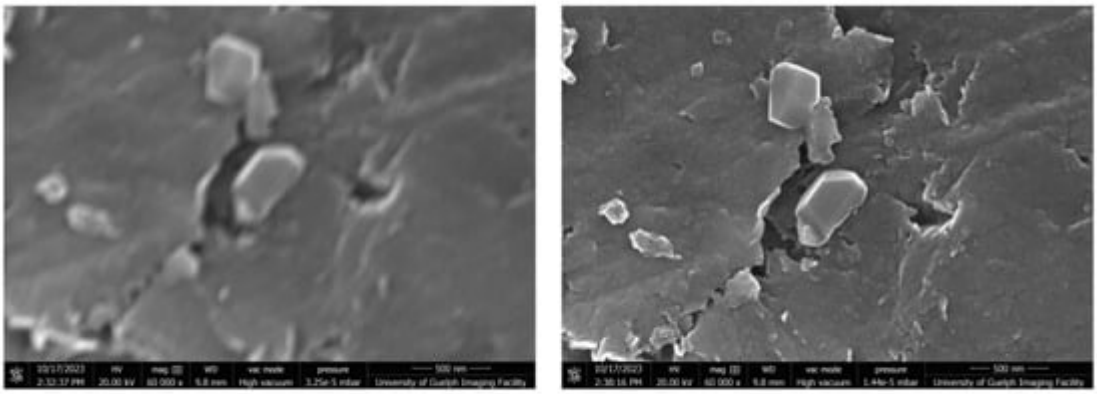

Figure 9. Comparison of the stigmator adjustment effect on wollastonite SEM images (**a**) before adjustment (**b**) after adjustment.

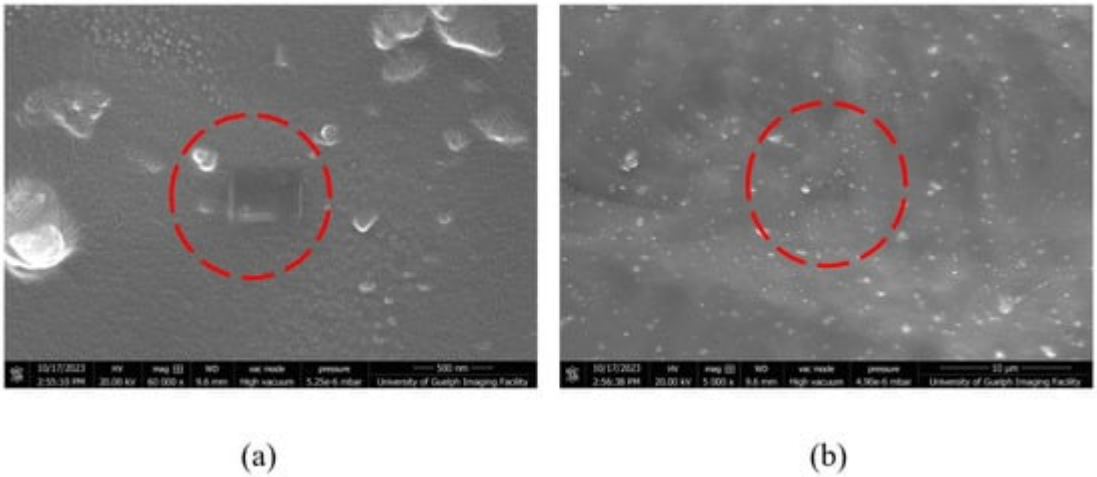

Figure 10. The effect of electron beam focusing on the sample for a longer period of time at (**a**) 60k× and (**b**) 5k× magnifications.

References

1. Li, C.; Wang, D.; Kong, L. Application of Machine Learning Techniques in Mineral Classification for Scanning Electron Microscopy—Energy Dispersive X-Ray Spectroscopy (SEM-EDS) Images. J. Pet. Sci. Eng. 2020, 200, 108178.
2. Wen, Y.; Cheng, Y.; Liu, Z.; Liu, C.; Nie, Q. Application of SEM and EDS for mineral composition of shale gas reservoir. IOP Conf. Ser. Mater. Sci. Eng. 2020, 780, 042055.
3. Nikonow, W.; Rammlmair, D. Automated mineralogy based on micro-energy-dispersive X-ray fluorescence microscopy (µ-EDXRF) applied to plutonic rock thin sections in comparison to a mineral liberation analyzer. Geosci. Instrum. Methods Data Syst. 2017, 6, 429–437.

4. Chalouati, S.; Yoosefdoost, A.; Chiang, Y.W.; Santos, R.M. Intensified mineral carbonation of natural Canadian silicates using simultaneous ball milling. Int. J. Coal Geol. 2023, 277, 104332.
5. Santos, R.M.; Knops, P.C.M.; Rijnsburger, K.L.; Chiang, Y.W. CO2 Energy Reactor—Integrated Mineral Carbonation: Perspectives on Lab-Scale Investigation and Products Valorization. Front. Energy Res. 2016, 4.
6. Lammers, K.; Murphy, R.; Riendeau, A.; Smirnov, A.; Schoonen, M.A.A.; Strongin, D.R. CO2 Sequestration through Mineral Carbonation of Iron Oxyhydroxides. Environ. Sci. Technol. 2011, 45, 10422–10428.
7. Haque, F.; Santos, R.M.; Chiang, Y.W. Using nondestructive techniques in mineral carbonation for understanding reaction fundamentals. Powder Technol. 2019, 357, 134–138.
8. Zarandi, A.E.; Larachi, F.; Beaudoin, G.; Plante, B.; Sciortino, M. Nesquehonite as a carbon sink in ambient mineral carbonation of ultramafic mining wastes. Chem. Eng. J. 2017, 314, 160–168.
9. Fantucci, H.; Sidhu, J.S.; Santos, R.M. Mineral Carbonation as an Educational Investigation of Green Chemical Engineering Design. Sustainability 2019, 11, 4156.
10. Ali, A.; Chiang, Y.W.; Santos, R.M. X-ray Diffraction Techniques for Mineral Characterization: A Review for Engineers of the Fundamentals, Applications, and Research Directions. Minerals 2022, 12, 205.
11. Klug, H.P.; Alexander, L.E. X-ray Diffraction Procedures: For Polycrystalline and Amorphous Materials, 2nd ed.; Wiley: Hoboken, NJ, USA, 1974; ISBN 978-0-471-49369-3.
12. Ali, A.; Mendes, C.E.; de Melo, L.G.T.C.; Wang, J.; Santos, R.M. Production of Sodium Bicarbonate with Saline Brine and CO2 Co-Utilization: Comparing Modified Solvay Approaches. Crystals 2023, 13, 470.
13. Chi, G.C.; Xiao, G.; Chen, Y.L.; Wu, Y.; Hu, J.-F.; Wang, H.-J.; Yue, M.-X.; Wang, X. Application of X-ray powder diffractometer in the identification and classification of phyllite. Geol. Resour. 2013, 22, 409–414.
14. Zhang, X.-h. Controlling factors of order degree of dolomite in carbonate rocks: A case study from lower palezoic in Tahe oilfield and Triassic in northeastern Sichuan basin. Lithol. Reserv. 2009, 21, 50–55.
15. Trindade, M.; Dias, M.; Coroado, J.; Rocha, F. Mineralogical transformations of calcareous rich clays with firing: A comparative study between calcite and dolomite rich clays from Algarve, Portugal. Appl. Clay Sci. 2009, 42, 345–355.
16. Dri, M.; Sanna, A.; Maroto-Valer, M.M. Mineral carbonation from metal wastes: Effect of solid to liquid ratio on the efficiency and characterization of carbonated products. Appl. Energy 2014, 113, 515–523.

17. Reynolds, B.; Reddy, K.J.; Argyle, M.D. Field Application of Accelerated Mineral Carbonation. Minerals 2014, 4, 191–207.
18. Newbury, D.E.; Ritchie, N.W.M. Is Scanning Electron Microscopy/Energy Dispersive X-ray Spectrometry (SEM/EDS) Quantitative? Scanning 2013, 35, 141–168.
19. Mandal, S.; Kumar, C.J.D.; Kumar, D.; Syed, K.; Van Ende, M.; Jung, I.; Finkeldei, S.C.; Bowman, W.J. Designing environment-friendly chromium-free Spinel-Periclase-Zirconia refractories for Ruhrstahl Heraeus degasser. J. Am. Ceram. Soc. 2020, 103, 7095–7114.
20. Warlo, M.; Wanhainen, C.; Bark, G.; Butcher, A.R.; McElroy, I.; Brising, D.; Rollinson, G.K. Automated Quantitative Mineralogy Optimized for Simultaneous Detection of (Precious/Critical) Rare Metals and Base Metals in A Production-Focused Environment. Minerals 2019, 9, 440.
21. Schulz, B.; Sandmann, D.; Gilbricht, S. SEM-Based Automated Mineralogy and its Application in Geo- and Material Sciences. Minerals 2020, 10, 1004.
22. Schulz, B.; Merker, G.; Gutzmer, J. Automated SEM Mineral Liberation Analysis (MLA) with Generically Labelled EDX Spectra in the Mineral Processing of Rare Earth Element Ores. Minerals 2019, 9, 527.
23. Smythe, D.M.; Lombard, A.; Coetzee, L.L. Rare Earth Element deportment studies utilising QEMSCAN technology. Miner. Eng. 2013, 52, 52–61.
24. Rollinson, G.K.; Andersen, J.C.Ø.; Stickland, R.J.; Boni, M.; Fairhurst, R. Characterisation of non-sulphide zinc deposits using QEMSCAN®. Miner. Eng. 2011, 24, 778–787.
25. Knappett, C.; Pirrie, D.; Power, M.; Nikolakopoulou, I.; Hilditch, J.; Rollinson, G. Mineralogical analysis and provenancing of ancient ceramics using automated SEM-EDS analysis (QEMSCAN®): A pilot study on LB I pottery from Akrotiri, Thera. J. Archaeol. Sci. 2011, 38, 219–232.
26. Saghiri, M.A.; Asgar, K.; Lotfi, M.; Karamifar, K.; Saghiri, A.M.; Neelakantan, P.; Gutmann, J.L.; Sheibaninia, A. Back-scattered and secondary electron images of scanning electron microscopy in dentistry: A new method for surface analysis. Acta Odontol. Scand. 2012, 70, 603–609.
27. Kjellsen, K.; Monsøy, A.; Isachsen, K.; Detwiler, R. Preparation of flat-polished specimens for SEM-backscattered electron imaging and X-ray microanalysis—Importance of epoxy impregnation. Cem. Concr. Res. 2003, 33, 611–616.
28. Santos, R.M.; Ling, D.; Sarvaramini, A.; Guo, M.; Elsen, J.; Larachi, F.; Beaudoin, G.; Blanpain, B.; Van Gerven, T. Stabilization of basic oxygen furnace slag by hot-stage carbonation treatment. Chem. Eng. J. 2012, 203, 239–250.
29. Heinrich, K.F.J.; Yakowitz, H. Quantitative electron probe microanalysis: Fluorescence correction uncertainty. Microchim. Acta 1968, 56, 905–916.

30. Duma, Z.-S.; Sihvonen, T.; Havukainen, J.; Reinikainen, V.; Reinikainen, S.-P. Optimizing energy dispersive X-Ray Spectroscopy (EDS) image fusion to Scanning Electron Microscopy (SEM) images. Micron 2022, 163, 103361.
31. Scimeca, M.; Bischetti, S.; Lamsira, H.K.; Bonfiglio, R.; Bonanno, E. Energy Dispersive X-ray (EDX) microanalysis: A powerful tool in biomedical research and diagnosis. Eur. J. Histochem. 2018, 62, 2841.
32. Kutchko, B.G.; Kim, A.G. Fly ash characterization by SEM–EDS. Fuel 2006, 85, 2537–2544.
33. Georget, F.; Wilson, W.; Scrivener, K.L. edxia: Microstructure characterisation from quantified SEM-EDS hypermaps. Cem. Concr. Res. 2020, 141, 106327.
34. Vermeij, E.; Zoon, P.; Chang, S.; Keereweer, I.; Pieterman, R.; Gerretsen, R. Analysis of microtraces in invasive traumas using SEM/EDS. Forensic Sci. Int. 2012, 214, 96–104.
35. Girao, A.V.; Caputo, G.; Ferro, M.C. Application of scanning electron microscopy-energy dispersive X-ray spectroscopy (SEM-EDS). Compr. Anal. Chem. 2017, 75, 153–168.
36. Avula, A.; Galor, A.; Blackwelder, P.; Carballosa-Gautam, M.; Hackam, A.S.; Jeng, B.; Kumar, N. Application of Scanning Electron Microscopy With Energy-Dispersive X-Ray Spectroscopy for Analyzing Ocular Surface Particles on Schirmer Strips. Cornea 2017, 36, 752–756.
37. Han, S.; Löhr, S.C.; Abbott, A.N.; Baldermann, A.; Farkaš, J.; McMahon, W.; Milliken, K.L.; Rafiei, M.; Wheeler, C.; Owen, M. Earth system science applications of next-generation SEM-EDS automated mineral mapping. Front. Earth Sci. 2022, 10, 956912.
38. Haque, F.; Santos, R.M.; Chiang, Y.W. Optimizing inorganic carbon sequestration and crop yield with wollastonite soil amendment in a microplot study. Front. Plant Sci. 2020, 11, 1012.
39. Butera, A.; Pascadopoli, M.; Gallo, S.; Lelli, M.; Tarterini, F.; Giglia, F.; Scribante, A. SEM/EDS Evaluation of the Mineral Deposition on a Polymeric Composite Resin of a Toothpaste Containing Biomimetic Zn-Carbonate Hydroxyapatite (microRepair®) in Oral Environment: A Randomized Clinical Trial. Polymers 2021, 13, 2740.
40. Santos, R.M.; Van Bouwel, J.; Vandevelde, E.; Mertens, G.; Elsen, J.; Van Gerven, T. Accelerated mineral carbonation of stainless steel slags for CO2 storage and waste valorization: Effect of process parameters on geochemical properties. Int. J. Greenh. Gas Control 2013, 17, 32–45.
41. Sukmara, S.; Suyanti; Adi, W.A.; Manaf, A.; Gunanto, Y.; Sitompul, H.; Izaak, M.; Jobiliong, E.; Sarwanto, Y. Mineral analysis and its extraction process of ilmenite rocks in titanium-rich cumulates from Pandeglang Banten Indonesia. J. Mater. Res. Technol. 2022, 17, 3384–3393.
42. Weerakoon, A.T.; Cooper, C.; Meyers, I.A.; Condon, N.; Sexton, C.; Thomson, D.; Ford, P.J.; Symons, A.L. Does dentine mineral change with anatomical location, microscopic site and patient age? J. Struct. Biol. X 2022, 6, 100060.

43. Jiang, Y.; Li, Y.; Liao, S.; Yin, Z.; Hsu, W. Mineral chemistry and 3D tomography of a Chang'E 5 high-Ti basalt: Implication for the lunar thermal evolution history. Sci. Bull. 2021, 67, 755–761.
44. Lastra, R. Seven practical application cases of liberation analysis. Int. J. Miner. Process. 2007, 84, 337–347.
45. Hoal, K.; Stammer, J.; Appleby, S.; Botha, J.; Ross, J.; Botha, P. Research in quantitative mineralogy: Examples from diverse applications. Miner. Eng. 2009, 22, 402–408.
46. Ford, F.D.; Wercholaz, C.R.; Lee, A. Predicting process outcomes for Sudbury platinum-group minerals using grade-recovery modeling from mineral liberation analyzer (MLA) data. Can. Mineral. 2012, 49, 1627.
47. Macdonald, M.; Adair, B.; Bradshaw, D.; Dunn, M.; Latti, D. Learnings From Five Years of On-Site Mla at Kennecott Utah Copper Corporation: (Myth Busters Through Quantitative Evidence…). In Proceedings of the 10th International Congress for Applied Mineralogy (ICAM); Springer: Berlin/Heidelberg, Germany, 2012; pp. 419–426.
48. Anderson, K.F.; Wall, F.; Rollinson, G.K.; Moon, C.J. Quantitative mineralogical and chemical assessment of the Nkout iron ore deposit, Southern Cameroon. Ore Geol. Rev. 2014, 62, 25–39.
49. Gäbler, H.-E.; Melcher, F.; Graupner, T.; Bahr, A.; Sitnikova, M.A.; Henjes-Kunst, F.; Oberthür, T.; Brätz, H.; Gerdes, A. Speeding Up the Analytical Workflow for Coltan Fingerprinting by an Integrated Mineral Liberation Analysis/LA-ICP-MS Approach. Geostand. Geoanalytical Res. 2011, 35, 431–448.
50. Lund, C.; Lamberg, P.; Lindberg, T. Practical way to quantify minerals from chemical assays at Malmberget iron ore operations—An important tool for the geometallurgical program. Miner. Eng. 2013, 49, 7–16.
51. Schulz, B. Polymetamorphism in garnet micaschists of the Saualpe Eclogite Unit (Eastern Alps, Austria), resolved by automated SEM methods and EMP–Th–U–Pb monazite dating. J. Metamorph. Geol. 2016, 35, 141–163.
52. Pszonka, J.; Schulz, B. SEM Automated Mineralogy applied for the quantification of mineral and textural sorting in submarine sediment gravity flows. Gospod. Surowcami Miner. Miner. Resour. Manag. 2023, 38, 105–131.
53. Wessels, R.; Kok, T.; van Melick, H.; Drury, M. Constraining P-T conditions using a SEM automated mineralogy based work-flow—An example from Cap de Creus, NE Spain. In Proceedings of the EGU General Assembly Conference 2022, Vienna, Austria, 23–27 May 2022.
54. Ranta, J.-P.; Cook, N.; Gilbricht, S. SEM-based automated mineralogy (SEM-AM) and unsupervised machine learning studying the textural setting and elemental association of gold in the Rajapalot Au-Co area, northern Finland. Bull. Geol. Soc. Finl. 2021, 93, 129–154.

55. Gu, Y. Automated scanning electron microscope based mineral liberation analysis. J. Miner. Mater. Charact. Eng. 2003, 2, 33–41.
56. King, R.; Schneider, C. Stereological correction of linear grade distributions for mineral liberation. Powder Technol. 1998, 98, 21–37.
57. Chiaruttini, C.; Piga, L.; Schena, G. An assessment of the efficiency of a stereological correction for recovering the volumetric grade of particles from measures on polished sections. Int. J. Miner. Process. 1999, 57, 303–322.
58. Fandrichi, R.; Schneider, C.; Gay, S. Two stereological correction methods: Allocation method and kernel transformation method. Miner. Eng. 1998, 11, 707–715.
59. Leigh, G.; Lyman, G.; Gottlieb, P. Stereological estimates of liberation from mineral section measurements: A rederivation of Barbery's formulae with extensions. Powder Technol. 1996, 87, 141–152.
60. Goodall, W.R.; Scales, P.J. An overview of the advantages and disadvantages of the determination of gold mineralogy by automated mineralogy. Miner. Eng. 2007, 20, 506–517.
61. Pirrie, D.; Rollinson, G.K. Unlocking the applications of automated mineral analysis. Geol. Today 2011, 27, 226–235.
62. Li, B.; Nie, X.; Cai, J.; Zhou, X.; Wang, C.; Han, D. U-Net model for multi-component digital rock modeling of shales based on CT and QEMSCAN images. J. Pet. Sci. Eng. 2022, 216, 110734.
63. Liu, Z.; Liu, D.; Cai, Y.; Qiu, Y. Permeability, mineral and pore characteristics of coals response to acid treatment by NMR and QEMSCAN: Insights into acid sensitivity mechanism. J. Pet. Sci. Eng. 2020, 198, 108205.
64. Lin, S.; Hou, L.; Luo, X. Shale Mineralogy Analysis Method: Quantitative Correction of Minerals Using QEMSCAN Based on MAPS Technology. Appl. Sci. 2022, 12, 5013.
65. Mason, J.; Lin, E.; Grono, E.; Denham, T. QEMSCAN® analysis of clay-rich stratigraphy associated with early agricultural contexts at Kuk Swamp, Papua New Guinea. J. Archaeol. Sci. Rep. 2022, 42, 103356.
66. Vickery, K.; Eckardt, F. A closer look at mineral aerosol emissions from the Makgadikgadi Pans, Botswana, using automated SEM-EDS (QEMSCAN®). South Afr. Geogr. J. 2020, 103, 7–21.
67. Andersen, J.C.; Rollinson, G.K.; Snook, B.; Herrington, R.; Fairhurst, R.J. Use of QEMSCAN® for the characterization of Ni-rich and Ni-poor goethite in laterite ores. Miner. Eng. 2009, 22, 1119–1129.
68. Blannin, R.; Frenzel, M.; Tuşa, L.; Birtel, S.; Ivăşcanu, P.; Baker, T.; Gutzmer, J. Uncertainties in quantitative mineralogical studies using scanning electron microscope-based image analysis. Miner. Eng. 2021, 167, 106836.

69. Benvie, B.; Chapman, N.M.; Robinson, D.J.; Kuhar, L.L. A robust statistical method for mineralogical analysis in geometallurgical diagnostic leaching. Miner. Eng. 2013, 52, 178–183.
70. Lastra, R.; Paktunc, D. An estimation of the variability in automated quantitative mineralogy measurements through inter-laboratory testing. Miner. Eng. 2016, 95, 138–145.
71. Guseva, O.; Opitz, A.K.; Broadhurst, J.L.; Harrison, S.T.; Becker, M. Characterisation and prediction of acid rock drainage potential in waste rock: Value of integrating quantitative mineralogical and textural measurements. Miner. Eng. 2021, 163, 106750.
72. Leigh, G.; Sutherland, D.; Gottlieb, P. Confidence limits for liberation measurements. Miner. Eng. 1993, 6, 155–161.
73. Evans, C.L.; Napier-Munn, T.J. Estimating error in measurements of mineral grain size distribution. Miner. Eng. 2013, 52, 198–203.
74. Mariano, R.A.; Evans, C.L. Error analysis in ore particle composition distribution measurements. Miner. Eng. 2015, 82, 36–44.
75. Leißnar, T.; Bachmann, K.; Gutzmer, J.; Peuker, U.A. MLA-based partition curves for magnetic separation. Miner. Eng. 2016, 94, 94–103.
76. Buchmann, M.; Schach, E.; Tolosana-Delgado, R.; Leißner, T.; Astoveza, J.; Kern, M.; Möckel, R.; Ebert, D.; Rudolph, M.; van den Boogaart, K.G.; et al. Evaluation of Magnetic Separation Efficiency on a Cassiterite-Bearing Skarn Ore by Means of Integrative SEM-Based Image and XRF–XRD Data Analysis. Minerals 2018, 8, 390.
77. Schach, E.; Buchmann, M.; Tolosana-Delgado, R.; Leißner, T.; Kern, M.; van den Boogaart, K.G.; Rudolph, M.; Peuker, U.A. Multidimensional characterization of separation processes—Part 1: Introducing kernel methods and entropy in the context of mineral processing using SEM-based image analysis. Miner. Eng. 2019, 137, 78–86.
78. Hannula, J.; Kern, M.; Luukkanen, S.; Roine, A.; Boogaart, K.v.D.; Reuter, M. Property-based modelling and simulation of mechanical separation processes using dynamic binning and neural networks. Miner. Eng. 2018, 126, 52–63.
79. Efron, B. Bootstrap Methods: Another Look at the Jackknife. Ann. Stat. 1979, 7, 1–26.
80. Chernick, M.R. Bootstrap Methods: A Guide for Practitioners and Researchers; Applied Probability and Statistics; Wiley: Hoboken, NJ, USA, 1999.
81. Chayes, F.A. Petrographic analysis by fragment counting; Part 1, The counting error. Econ. Geol. 1944, 39, 484–505.
82. Chayes, F. Petrographic analysis by fragment counting; Part II, Precision of microsampling and the combined error of sampling and counting. Econ. Geol. 1945, 40, 517–525.

83. Plas, L.V.D.; Tobi, A.C. A chart for judging the reliability of point counting results. Am. J. Sci. 1965, 263, 87–90.
84. Parian, M.; Lamberg, P.; Mockel, R.; Rosenkranz, J. Analysis of mineral grades for geometallurgy: Combined element-to-mineral conversion and quantitative X-ray diffraction. Miner. Eng. 2015, 82, 25–35.
85. Jackson, B.R.; Reid, A.F.; Wittenberg, J.C. Rapid production of high quality polished sections for automated image analysis of minerals. Proc. Aust. Inst. Min. Metall. 1984, 289, 93–97.
86. Rahfeld, A.; Gutzmer, J. MLA-Based Detection of Organic Matter with Iodized Epoxy Resin—An Alternative to Carnauba. J. Miner. Mater. Charact. Eng. 2017, 5, 198–208.
87. O'brien, G.; Gu, Y.; Adair, B.; Firth, B. The use of optical reflected light and SEM imaging systems to provide quantitative coal characterisation. Miner. Eng. 2011, 24, 1299–1304.
88. Gomez, C.O.; Strickler, D.W.; Austin, L.G. An iodized mounting medium for coal particles. J. Electron Microsc. Tech. 1984, 1, 285–287.
89. Alim, A.; Abdullah, M.Z.; Aziz, M.S.A.; Kamarudin, R.; Gunnasegaran, P. Recent Advances on Thermally Conductive Adhesive in Electronic Packaging: A Review. Polymers 2021, 13, 3337.
90. Yuan, W.; Xiao, Q.; Li, L.; Xu, T. Thermal conductivity of epoxy adhesive enhanced by hybrid graphene oxide/AlN particles. Appl. Therm. Eng. 2016, 106, 1067–1074.
91. Grundmann, G.; Scholz, H. Preparation Methods in Mineralogy and Geology: The Preparation of Thin Sections, Polished Sections, Acetate Foil Prints, Preparation for Elutriation Analysis and Staining Tests for the Optical and Electron Microscopy; Technical University of Munich: Munich, Germany, 2015.
92. Rodríguez, J.-R.; Turégano-López, M.; DeFelipe, J.; Merchán-Pérez, A. Neuroanatomy from Mesoscopic to Nanoscopic Scales: An Improved Method for the Observation of Semithin Sections by High-Resolution Scanning Electron Microscopy. Front. Neuroanat. 2018, 12, 14.
93. Ren, H.; Zhang, X.; Li, Y.; Zhang, D.; Huang, F.; Zhang, Z. Preparation of Cross-Sectional Membrane Samples for Scanning Electron Microscopy Characterizations Using a New Frozen Section Technique. Membranes 2023, 13, 634.